Acta Astronautica 226 (2025) 570–584

Contents lists available at ScienceDirect

Acta Astronautica

journal homepage: www.elsevier.com/locate/actaastro

Methodology for robust analysis of bolts slippage in cryogenic space missions

Alejandro Fernández-Soler [a,*], Andrés García-Pérez [a], Gianluca Morgante [b], Javier Pérez-Álvarez [a], Gustavo Alonso [a], Laura García-Moreno [a], Antonio Scippa [c], Daniele Gottini [c], Ciro Del Vecchio [d]

[a] Instituto Universitario de Microgravedad "Ignacio Da Riva" (IDR), Escuela Técnica Superior de Ingeniería Aeronáutica y del Espacio (ETSIAE), Universidad Politécnica de Madrid (UPM), Pza. Cardenal Cisneros 3, 28040, Madrid, Spain
[b] Istituto Nazionale di Astrofisica (INAF), Osservatorio di Astrofisica e Scienza dello Spazio (OAS), via Piero Gobetti 93/3, 40129, Bologna, Italy
[c] Dipartimento di Ingegneria Industriale, Università degli Studi di Firenze (UniFI), via St Marta 3, I-50139, Florence, Italy
[d] Istituto Nazionale di Astrofisica (INAF), Osservatorio Astrofisico di Arcetri (OAA), Largo E. Fermi 5, 50125, Florence, Italy

ARTICLE INFO

Keywords:
Slippage
Primary mirror
ARIEL
STOP analysis
Thermal analysis
Thermoelastic analysis
Cooldown
Cryogenic space telescope

ABSTRACT

The assessment of slippage in cryogenic space missions is fundamental from a mechanical point of view as it is one of the main failure modes of a bolt in a mechanical interface. It is usually performed on the basis of temperature maps obtained from the worst-case thermal design cases, with particular interest in the transient case during the cooldown. Traditionally, the thermal mapping has to be transferred to the detailed FEM model. This process requires a lot of interaction between the thermal and structural disciplines, which is often not easy. Moreover, the thermal mapping usually corresponds to the instant of maximum gradient between the clamped parts along the transient case. In this paper, a new methodology is proposed to speed up the evaluation of the temperature effect on the slippage from an analytical model correlated with the FEM model. Then, the interactions between the structural and the thermal responsible may be reduced. In addition, the proposed methodology evaluates the entire temperature curve of the transient case, rather than a single instant. In this way, the thermal effect on slippage can be evaluated in a robust and agile process, facilitating the definition of requirements in terms of the maximum allowable temperature gradient as a function of preload or vice versa. This methodology has been validated with the primary mirror of the ARIEL mission, which is a cryogenic European mission that aims to study exoplanets by making observations from a thermally stable orbit at L2 point of the Sun-Earth system. Therefore, the correct design of the primary mirror is essential for the successful science observations of the mission.

Nomenclature

A_{eq}	Equivalent cross-sectional area at the clamped parts [m^2]
A_i	Cross-sectional area [m^2]
CTE_b	Secant coefficient of thermal expansion of the bolt [K^{-1}]
CTE_{c1}	Secant coefficient of thermal expansion of the clamped part 1 [K^{-1}]
E_c	Young's Modulus [GPa]
E_{eq}	Equivalent Young Modulus [GPa]
F_A	Axial force [N]
F_Q	Shear force [N]
$F^T_{V,min}$	Minimum preload at reference temperature [N]
$F_{V,min}$	Remaining minimum preload [N]
L_c	Length of the clamped part 1 [m]

(*continued on next column*)

(*continued*)

L_0	Initial length [m]
T_{ref}	Reference temperature [K]
T_1	Temperature clamped part 1 [K]
T_2	Temperature clamped part 2 [K]
sf_{slip}	Safety factor [−]
ΔT_{lim}	Maximum allowable gradient temperature between the clamped parts [K]
ΔT_{TH}	Maximum gradient temperature between the clamped parts [K]
δ_C	Compliance of the clamped parts [m N^{-1}]
δ_b	Compliance of the bolt [m N^{-1}]
ε	Infrared emissivity [−]
ε^{MEC}	Mechanical strain [−]
ε^{TH}	Thermoelastic strain [−]

(*continued on next page*)

* Corresponding author.
E-mail address: alejandrojose.fernandez@upm.es (A. Fernández-Soler).

https://doi.org/10.1016/j.actaastro.2024.10.048
Received 4 July 2024; Received in revised form 3 September 2024; Accepted 19 October 2024
Available online 28 October 2024

(*continued*)

μ_S	Friction coefficient between the clamped parts [−]
ϕ_N	Force ratio [−]

Abbreviations

ACS	Active Cooler System
AIRS	ARIEL Infra-Red Spetrometer
ARIEL	Atmospheric Remote-sensing Infrared Exoplanet Large-survey
B1	Baffle Mirror 1
CTE	Coefficient of thermal expansion
ECSS	European Cooperation for Space Standardization
ESA	European Space Agency
FEM	Finite Element Model
FGS	Fine Guidance System
FH	Flexure Hinge
FPE	Focal Plane Electronics
GMM	Geometrical Mathematical Model
I/F	Interface
JAXA	Japanese Space Agency
LPM	Lumped Parameters Method
M1	Mirror 1
M2	Mirror 2
M2M	M2 Refocus Mechanism
M3	Mirror 3
M4	Mirror 4
MLI	Multi-Layer Insulation
NASA	National Aeronautics Space Administration
NIST	National Institute of Standards and Technology
PA	Product Assurance
PIP	Payload Interface Plate
PLM	Payload Module
STOP	Structural-Thermal-Optical Performance
SVM	Service Module
TA	Telescope Assembly
TMM	Thermal Mathematical Model
TMS	Telescope Metering Structure
TOB	Telescope Optical Bench
VG	V-Groove

1. Introduction

In recent decades, there has been a growing interest in the development of space telescopes to observe the cosmos, other planets, etc [1–5]. Advances in scientific observations allow to obtain a very good resolution, improving the quality of the information obtained. These observations require cryogenic operational temperatures and, depending on the type of detectors, the operational temperature range of the observation can be in the order of a few ∼ K or even lower ∼ mK [6]. At cryogenic temperature, the mechanical properties of the materials change with regard to those of the room temperature. This fact leads to deformation on the structural parts relative to its dimensions at room temperature. Therefore, the thermo-mechanical design is essential for the correct functionality of the different optical elements.

Traditionally in space missions, the effect of the thermoelastic phenomena in the optics behaviour is evaluated through the design process named STOP (Structural-Thermo-Optical-Performance) analysis [7,8]. This process consists of assessing the effect of temperature variation on structural deformation, and its subsequent effect on the expected optical path. Hence, this analysis process involves the exchange of information between the thermal, structural and optical engineers. Each of them works with different specific software (e.g. ESATAN-TMS, NASTRAN-PATRAN and ZEMAX for the thermal, structural and optical engineers respectively), and usually belongs to different institutions. Then, data exchange requires a management effort for all the involved parties.

From a mechanical point of view, one of the main failure modes of a bolt in an I/F is the transverse slippage between the clamped parts due to transverse load [9]. The transverse loads at the interfaces caused by thermoelastic effects appear when there is a difference in the temperature or a difference in the Coefficient of thermal expansion (CTE) between the clamped parts. The risk of slippage increases when the preload loss associated with the temperature gradient between the clamped parts is too large. Thus, the slippage phenomena will depend on the type of joint in the I/F, the temperature difference between the clamped parts, and the absolute temperature at which it occurs. Therefore, the maximum preload applied at the I/F must be sufficient to ensure that the loss of preload associated with the temperature gradient does not cause slippage.

Hence, one of the cases to be analysed is the cooling phase of the telescope, e.g. during its journey from its parking orbit on Earth to its final orbit (e.g. L2). During this phase, the temperature of the elements goes from room temperature to operational temperatures., and then, it is critical to analyse the temperature gradients between the different mechanical joints.

In the design phase, this slippage worst-case is usually analysed by obtaining the temperature map corresponding to the instant at which the maximum ΔT between interfaces occurs, and transferring this temperature map from the thermal model to the structural model [8,10,11]. However, since the loss of preload depends not only on the thermal gradient itself, but also on the temperature at which the gradient occurs, it cannot be guaranteed that the slippage worst-case will occur at the instant of maximum temperature gradient. In addition, the clamped parts are usually mechanically assembled in different bolted areas (i.e. two parts are mechanically connected with more than one interface), and then the maximum temperature gradient at each I/F may not be necessary at the same time. Therefore, to make a robust assessment of the impact of the temperature gradient during a transient thermal case on the mechanical behaviour of the bolts, it may not be sufficient to analyse only the time instant of maximum gradient between the two clamped parts of an I/F, but the entire cooldown period.

Hence, this paper presents the new methodology followed to analyse the slippage worst-case of a cryogenic mirror, demonstrated through application to the Primary Mirror of ARIEL mission [12,13] during the cooldown transient case.

The ARIEL mission is planned to be launched in 2029 from French Guiana aboard Ariane 6.2 [12]. Its primary scientific objective is to study exoplanets to better understand their evolution, formation, and the composition of their atmospheres.

The ARIEL spacecraft consists of two separated and thermally decoupled modules as it shown in Fig. 1: the service module (SVM), which houses all the electronics and the cooler compressor, and the cold Payload Module (PLM). The structure of the PLM is based on a horizontal telescope configuration, and comprises an off-axis Cassegrain telescope [14].

The PLM has been designed to ensure that both the scientific instruments and the telescope assembly (TA), consisting of Mirror 1, Mirror 2, the M2 mechanism, Mirror 3, Mirror 4, the baffle, and the TA structure, which includes the metering structure, struts, and the optical bench (TOB), operate at temperatures below 60 K [15]. This is achieved using a combination of active and passive thermal elements. The passive system includes radiators and three V-grooves mechanically supported on the SVM by insulating struts. These V-grooves efficiently reject heat to the cold space, intercepting parasitic heat leaks from sources such as the harness or the active cryocooler. The last V-Groove, VG3, defines the coldest passive environment for the TA and instruments accommodated on the PLM. Additionally, the telescope assembly, along with the baffle and the optical bench, which are black-painted, act as radiating surfaces, enhancing the PLM's thermal performance.

The content of the paper is organised as follows: in section 2, the analytical model proposed to evaluate the slippage is deeply described. In section 3, a detailed step-by-step explanation of the thermoelastic analysis is presented. After that, the methodology is applied to the Primary Mirror of ARIEL mission, with special explanation to the Primary Mirror I/F and the thermal and Finite Element Models, and summarizing the results in section 4. Finally, the conclusions and the main lessons

Fig. 1. ARIEL spacecraft overview (left) and PLM overview (right).

learned are presented in order to help the community in future space missions' applications in section 5.

2. Analytical model for slippage calculation caused by thermoelastic shear forces

The remaining minimum preload, $F^T_{V,min}$, after considering its loss caused by the decrease of temperature can be estimated according to the handbook of threaded fasteners of the European Standards [9]:

$$F^T_{V,min} = F_{V,min} + \frac{L_c}{\delta_c + \delta_b}(CTE_{c1} - CTE_b)(T_1 - T_{ref}), \quad (1)$$

where the involved parameters are defined in Table 1.

The clamped part 1 is the part in contact with the head of the bolt (through the corresponding washer), while the part 2 contains the female thread (see Fig. 2). Therefore, the length, CTE and temperature that appear in Eq. (1) correspond to parameters associated to the clamped part 1, which is the part directly affected by the compression zone of the bolt, and thus, with influence on the thermoelastic loss of preload. The decrease of the minimum preload is produced during a cooldown ($T_1 < T_{ref}$) when the CTE of the bolt material (CTE_b) is lower than the CTE of the clamped part 1 ($CTEc_1$).

In this paper, the CTE parameters are defined as temperature-dependent functions. The secant CTE functions have been extracted from the NIST approach [16], which are based on polynomial expressions where the constants b, c, d and e depend on the material:

$$CTE_{ci} = b + c(T_i + T_{ref}) + d(T_i^2 + {T_{ref}}^2 + T_i T_{ref}) + e(T_i + T_{ref})(T_i^2 + {T_{ref}}^2). \quad (2)$$

The values for the constants of the CTE functions for the materials of the clamped parts (mostly aluminium 6061) and the bolts (steel, Inconel, titanium) are shown in Table 2, and the resulting secant CTE functions considering $T_{ref} = 293$ K are represented in Fig. 3.

The equation defined in the ECSS Threaded fastener handbook [9] to determine the individual slippage margin of safety (MoS_{slip}) of a bolt subjected to a combination of a shear force (F_Q) and an axial force (F_A) is given by:

Table 1
Definition of the parameters for Eq. (1).

Symbol	Description	Units
$F_{V,min}$	Minimum preload at reference temperature	N
L_c	Length of the clamped part 1	m
δ_C	Compliance of the clamped parts	m/N
δ_b	Compliance of the bolt	m/N
CTE_{c1}	Secant coefficient of thermal expansion of the clamped part 1	K^{-1}
CTE_b	Secant coefficient of thermal expansion of the bolt	K^{-1}

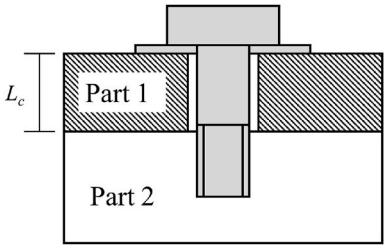

Fig. 2. Scheme of an insert joint composed of a bolt that connect two clamped parts.

Table 2
Values of the constants for the CTE functions for different materials.

Constant	Al 6061-T6	Ti 6Al 4V	Steel 316	Inconel 718
b [K^{-1}]	−3.0389E-06	−2.1400E-06	−3.9811E-06	−2.1200E-06
c [K^{-2}]	8.7696E-08	4.8070E-08	9.2683E-08	5.4970E-08
d [K^{-3}]	−9.9821E-11	−7.1110E-11	−2.0261E-10	−6.8820E-11
e [K^{-4}]	0.0	0.0	1.7127E-13	0.0

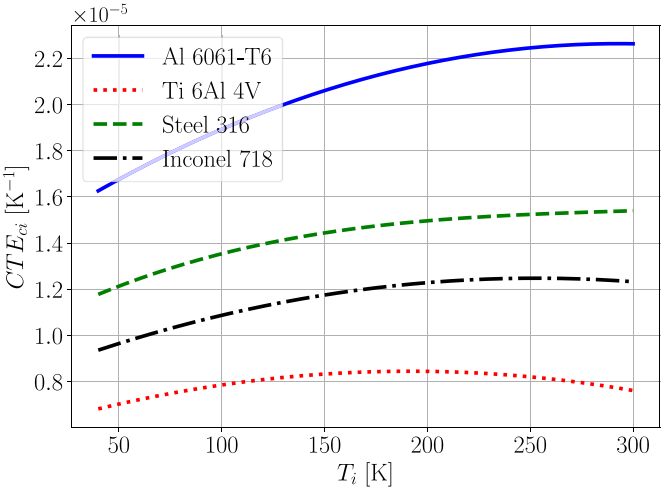

Fig. 3. Temperature-dependent secant CTE functions for different structural materials.

$$MoS_{slip} = \frac{\left[F^{T}_{V,min} - (1-\Phi_n)F_A\right]\mu_s}{sf_{slip}|F_Q|} - 1 \tag{3}$$

where sf_{slip} is a safety factor (recommended value is 1.25 [9]), Φ_n is the force ratio defined in Eq. (4), and μ_S is the friction coefficient between the clamped parts. Then, Eq. (3) shall be positive to avoid individual slippage.

$$\Phi_n = \frac{1}{2}\frac{\delta_c}{\delta_c + \delta_b} \tag{4}$$

In simple systems consisting of two clamped parts joined together at a single interface plane by various bolts, the generated thermoelastic I/F forces are in-plane, that is, shear forces, while the external axial forces F_A are zero. For a complex structure with more than two parts, the external axial force F_A at each screw appears as a result of interaction with other parts, non-homogenous temperature distribution and geometric complexity. In this study, the different numerical simulations performed with the model of the ARIEL main mirror reveal that the axial force F_A changes with non-monotonic dependence on ΔT and is less markedly than F_Q. Therefore, for each I/F analysed in this work, the axial force F_A is set to a representative constant value based on the order of magnitude according to the ΔT range analysed (see section 4.3).

A simple model to estimate the relationship between the shear forces, (F_Q), generated at the joining elements that connect two pieces has been defined. This simple model aims to have analytical equations that take into account the effect of joint type and the temperature of each piece to evaluate the shear forces. It consists of 2 bars with the same initial length (L_0) at a reference temperature (T_{ref}) as it is shown in Fig. 4. Both bars may be made of different materials with their corresponding Young's Modulus (E_{ci}), Coefficients of Thermal Expansion (CTE_{ci}), and with different cross-sectional areas (A_i). Both bars are clamped at the left end and joined to each other by a joining element at their free edges, which guarantees that both bars expand/contract equally, generating a pair of opposite forces (F_Q), each applied to each bar, which depend on the differences between the CTEs and the final temperatures.

Considering that after the temperature change from T_{ref} to T_1 for Bar 1 and T_2 for Bar 2, the total strains of both bars are the same [17]:

$$\varepsilon_1^{TOT} = \varepsilon_2^{TOT} = \varepsilon^{TOT} = \frac{\Delta L}{L_0}. \tag{5}$$

The total strain for each bar can be decomposed by the sum of the thermoelastic strain (ε^{TH}) and the mechanical strain (ε^{MEC}):

$$\varepsilon_1^{TH} + \varepsilon_1^{MEC} = \varepsilon_2^{TH} + \varepsilon_2^{MEC}. \tag{6}$$

Considering that both bars only deform in axial direction, each strain is substituted by its corresponding equation:

$$CTE_{c1}(T_1 - T_{ref}) + \frac{F_Q}{A_1 E_{c1}} = CTE_{c2}(T_2 - T_{ref}) - \frac{F_Q}{A_2 E_{c2}}. \tag{7}$$

The I/F force, F_Q, can be expressed as a function of the final temperatures T_1 and T_2:

$$F_Q = \frac{A_1 A_2 E_{c1} E_{c2}}{A_1 E_{c1} + A_2 E_{c2}}\left[CTE_{c2}(T_2 - T_{ref}) - CTE_{c1}(T_1 - T_{ref})\right], \tag{8}$$

or as a function of T_1 and $\Delta T = T_2 - T_1$:

$$F_Q = A_{eq}E_{eq}\left[(CTE_{c2} - CTE_{c1})(T_1 - T_{ref}) + CTE_{c2}\Delta T\right], \tag{9}$$

where the product $A_{eq}E_{eq}$ is defined by:

$$A_{eq}E_{eq} = \frac{A_1 A_2 E_{c1} E_{c2}}{A_1 E_{c1} + A_2 E_{c2}}. \tag{10}$$

Eq. (9) can be used to estimate the maximum shear force generated on the bolts that connect two parts subjected to a change of temperature. This equation shows better the two main contributions for the generated force. The first term inside the brackets represents the effect of the difference between the CTEs, which may come from the use of different materials between the clamped parts. The impact on the generated force may be significant if their CTEs are very different. However, when both clamped parts are made of the same material, the difference between the CTEs may come from the dependency with the temperature that these coefficients may have. The second term represents the generation of shear forces caused by the temperature differences (gradient) between the two connected parts. The sum of both terms is multiplied by the product of the equivalent cross-sectional area (A_{eq}) and the equivalent Young's Modulus (E_{eq}), which represent scale factors that amplify the generated force for high values of these parameters.

Hence, taking into account the dependency with the temperature of the shear force, F_Q, from Eq. (9) and the minimum preload, $F_{V,min}$, given in Eq. (1), the margin of safety on individual slippage is given by:

$$MoS_{slip} = \frac{\left[F_{V,min} + \frac{L_c}{\delta_c+\delta_b}(CTE_{c1} - CTE_b)(T_1 - T_{ref}) - (1-\Phi_n)F_A\right]\mu_s}{sf_{slip}A_{eq}E_{eq}\left|CTE_{c2}(T_2 - T_{ref}) - CTE_{c1}(T_1 - T_{ref})\right|} - 1 \tag{11}$$

The maximum allowable temperature difference between both clamped parts (ΔT_{lim}) to avoid individual slippage is obtained by equalling to zero the margin of safety on slippage. This temperature difference is obtained as an implicit function with any of the temperatures of the clamped parts as independent variable. In this work, the temperature of the clamped part 1 has been considered as the independent variable, giving an implicit expression of the following type:

$$\Delta T_{lim} = f(T_1) \tag{12}$$

Note that Eq. (1) is derived under the assumption that the bolt and the clamped part 1 remains at the same temperature [9]. However, this assumption may not be necessarily true in all the interfaces. To address this, the bolt can be assumed to be at the same temperature as the clamped part 2 (a conservative approach). Then, an additional term would be added to Eq. (1), similar to the last term in Eq. (9).

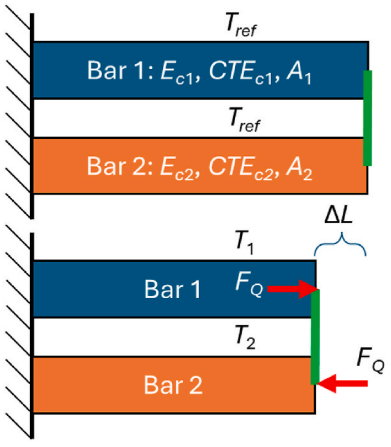

Fig. 4. Analytical scheme of two connected bars of different materials and temperatures under a decrease of temperature.

3. Thermoelastic analysis methodology

This section presents the proposed methodology to robustly analyse the mechanical worst-case of a cryogenic space mission primary mirror from a slippage point of view.

Unlike the standard approach of evaluating a small set of critical thermoelastic load cases [6,18], which are typically the extreme steady-state thermal situations (hot and cold operational and non-operational load cases), and sometimes a transient case with the

maximum gradient between two parts, this work proposes an alternative approach for the transient case. It consists of evaluating the entire cooldown process to guarantee that there is not slippage at any moment that can provoke misalignment in the optical elements. By the analytical approach described in section 2, the maximum allowable temperature gradient between the two clamped parts to avoid slippage is related to the absolute temperature of one of these two parts. Then, the comparison between the resulting curve ($\Delta T_{lim} = f(T_1)$) and the evolution of the temperature gradient obtained by the thermal analysis during the cooldown ($\Delta T_{TH} = f(T_1)$) can be easily performed. Therefore, it can be determined graphically if the slippage is avoided with the selected preload for the thermal gradient expected during the cooldown. Additionally, the minimum preload, $F_{V,min}$, that avoids slippage can be quickly determined with the proposed approach (Eq. (11)). And, on the contrary, the maximum thermal gradient that avoids slippage with the maximum preload selected can be determined.

The full flowchart diagram is summarized in Fig. 5. First, the structural FEM (Finite Element Model) and thermal model (based on the Lumped Parameter Method (LPM)) are built. First, from the thermal model, the cooling transient case from room temperature to cryogenic temperature is analysed to obtain the profiles of the temperature variation in each I/F with time. Then, at each interface, the time instant at which the maximum temperature difference occurs is determined. Besides, it is essential to carry out a sensitivity analysis of the different thermal parameters that have an impact on the thermal dynamic response, especially in the initial design phases. In parallel, the A_{eq} parameter of the simple analytical model for each evaluated I/F (see section 2) is correlated with the FEM results based on the comparison between the analytical and the numerical shear forces.

Then, the maximum ΔT that guarantees no slippage is determined with the correlated simple analytical model. It is based on the applied preload and the temperature profile of the coolest clamped parts at which this ΔT occurs, defining a potential valid design region. Therefore, it is possible to define a thermal requirement in terms of maximum ΔT allowable at each I/F.

Finally, as a validation of the results, the temperature map obtained at the certain critical instant for the thermal transient case (typically the maximum gradient between the two clamped parts), is transferred to the detailed FEM, and the thermoelastic case is evaluated to confirm that the bolt preload selected prevents slippage at any interface under study.

4. ARIEL primary mirror slippage study case

As mentioned above, the methodology presented in this paper will be applied to the Primary Mirror (M1) of ARIEL mission. M1 consists of an elliptical monolithic piece of aluminium EN AW 6061 T651 with aperture dimensions of 1.1 m × 0.7 m.

M1 is mounted on the Telescope Optical Bench (TOB) by three Flexure Hinges (FH) as it is shown in Fig. 6, one at the top and the two others located at the laterals bottom. The aim of the Flexure Hinges, also manufactured on EN AW 6061 T651 aluminium, is to decouple the different thermoelastic deformations expected between the M1 and the TOB. Each Flexure Hinge is mechanically attached to the M1 by two interfaces. Each interface consists of M8 x 6 Inconel 718 stud bolts. In addition, each Flexure Hinge is mechanically attached to the TOB by M12 x 2 Inconel 718 stud bolts. In all interfaces, CuSn 6 helicoils are used since the *CTE* is quite similar to the aluminium one.

The M1-FH I/F is based on high planarity with very low roughness contact that ensures a good thermal conductive coupling. The FH-TOB I/F is based on hemispherical joint to compensate the effects of manufacturing tolerances. The CAD view of both interfaces is shown in Fig. 7.

In this section, the methodology described in Section 3 is applied to the ARIEL Primary Mirror. First, the structural and thermal models of the ARIEL PLM are explained in section 4.1. After that, the cooldown thermal cases and the results in terms of temperature are deeply explained in section 4.2. Then, the simple analytical model is correlated with the detailed FEM in section 4.3. The study of the effect of the preload force selected with the temperature from a slippage point of view is evaluated in section 4.4. Then, the preload force selection that

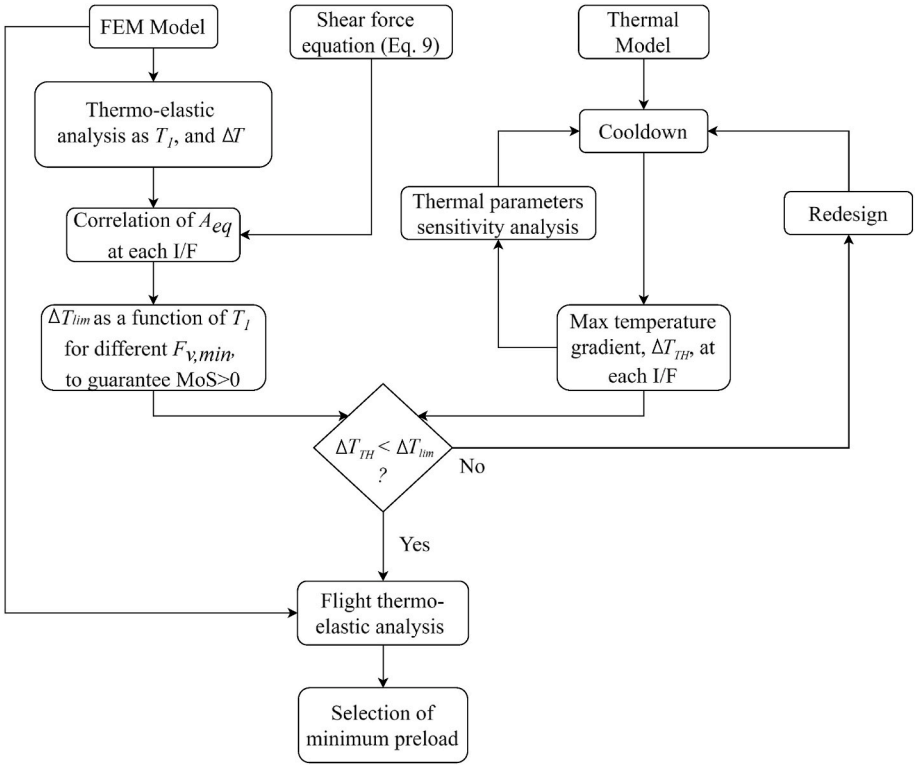

Fig. 5. Flowchart of the thermoelastic analysis.

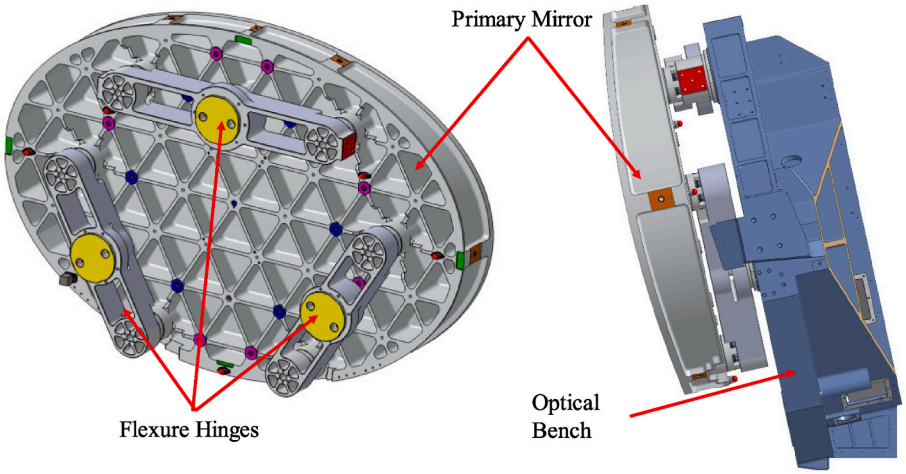

Fig. 6. Overview of the primary mirror, M1 Flexure hinges and optical bench CAD.

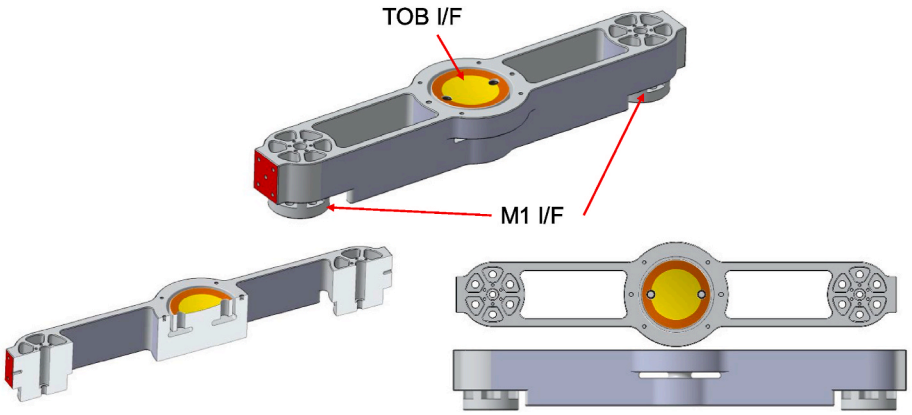

Fig. 7. Isometric and section view of the Flexure Hinge CAD.

ensures the slippage prevent for the ARIEL Primary Mirror is presented in section 4.5. Finally, in section 4.6, the preload selected is validated with the thermal maps obtained from the thermal analysis.

4.1. ARIEL structural and thermal models

In this section, the thermal and structural models of the ARIEL PLM are deeply explained.

4.1.1. Thermal model of ARIEL PLM

The Telescope Assembly consists of the Optical Bench (TOB), the Metering Structure (TMS), the struts, the mirrors (M1, M2, M3, and M4), the M2 Refocus Mechanism (M2M), the M1 Baffle (B1) and the M2 Baffle (B2). All these elements are made of Al-6061. All the surfaces (except for the mirrors and the M2M) are black painting not only due to optics reasons but also to maximise the radiative heat exchange with the space heat sink. The TA Geometrical Mathematical Model (GMM) is shown in Fig. 8.

The M1 thermal behaviour is driven by the TOB, as the M1 is mounted on the TOB through three Al-6061 Flexure hinges, as above commented. The TOB, which is a huge Al-6061 piece of ~ 90 kg, is conductively coupled to the B1 and to the Instrument Radiator, to reject all the heat leakages provided from the instrumentation allocated on the TOB instrument cavity.

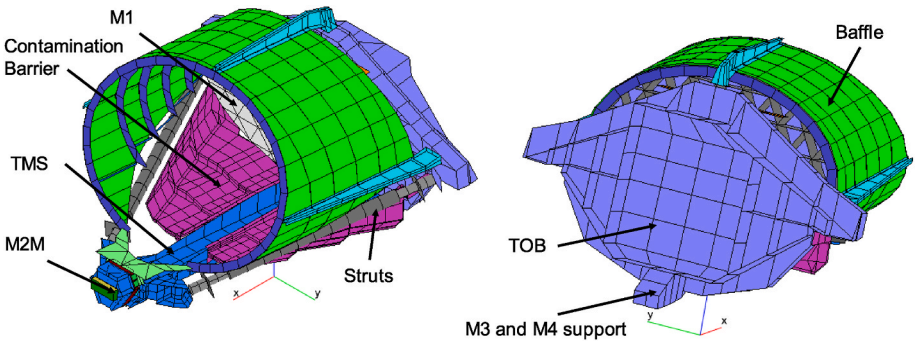

Fig. 8. Front and rear view of the Telescope Assembly GMM.

From the thermo-mechanical point of view, the three Flexures Hinges that support the mirror on the TOB play an important role as they define the thermal coupling to the bench. This shall be good enough to minimize the thermal gradient with the TA structure. The GMM of the M1 and the Flexure Hinges is shown in Fig. 9.

The conductive coupling between the M1 and the Flexure Hinges has been estimated based on the contact area and by defining a thermal contact coefficient. The conductive coupling between the Flexure Hinge and TOB has been modelled in the same way, but taking into account that the contact at this joint is based on a convex contact surface, as previously commented in section 4.

As the thermal behaviour of the M1 is leading by the conductive coupling between the TOB through the FH, sensitivity analyses have been performed to study the effect of the conductive coupling uncertainty on the M1 thermal behaviour (see section 4.2).

4.1.2. Finite element model of the ARIEL PLM

The complete finite element model (FEM) of the ARIEL PLM (see Fig. 10) is mostly composed of 3D elements to represent the main structural parts. Due to the complex geometry of these parts, the predominant element type is tetrahedral with 10 nodes each. M1 mirror and its flexure hinges are modelled by 3D hexahedral and wedge-type elements. Those parts considered with thin thickness such as the main Baffle and the M2M are modelled by 2D quadrilateral elements. The ARIEL PLM FEM contains a total of more than two million nodes. The approach used to model the bolts is by the combination of two RBE2 rigid elements, each one attached to each connected part, whose centre nodes are joined by a zero-length CBUSH element.

The work here presented focuses on the calculation of the interface forces on the elements that represent the bolts that connect the principal M1 mirror with its flexure hinges and between these hinges and the Optical Bench. A FEM with only these parts and their connecting elements (see Fig. 11) will be analysed in several load cases considering different temperatures combinations and with isostatic boundary conditions.

The backside of the M1 mirror with its three flexure hinges is shown in Fig. 12.

The results of interest are the forces calculated at the interface elements (CBUSH). The joint between each flexure hinge and the TOB is composed by two bolts located at the centre of the flexure hinge, where the numbering used for the representing CBUSH elements is shown in Fig. 13.

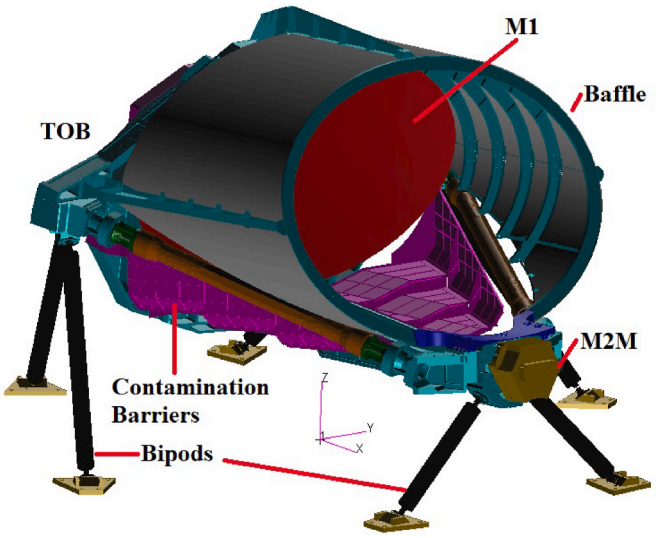

Fig. 10. Fem of the ariel plm.

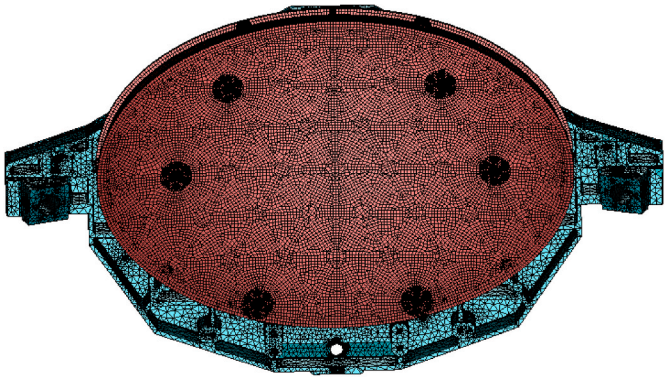

Fig. 11. FEM of the Optical Bench, M1 mirror and its flexure hinges.

4.2. Cooldown thermal case

During the journey from the parking orbit on Earth to L2, where ARIEL will operate, the cooling phase takes place. During this stage, the temperature of the equipment drop from ambient to operational temperatures. In particular, the TA reaches ~50 K. In addition, at this stage, a decontamination scenario of the optical elements is foreseen, so the cooling is interrupted by switching on the decontamination heaters to reach the decontamination lines set point. Hence, the temperature of the critical optical elements is maintained at 170 K to remove the possible deposit of contaminants on the optics surface [19].

During the first cooling stage, the different subsystems temperature rate of change is expected to be higher, as the radiative coupling with the space heat sink (~3 K) is higher. This fact is explained by two reasons:

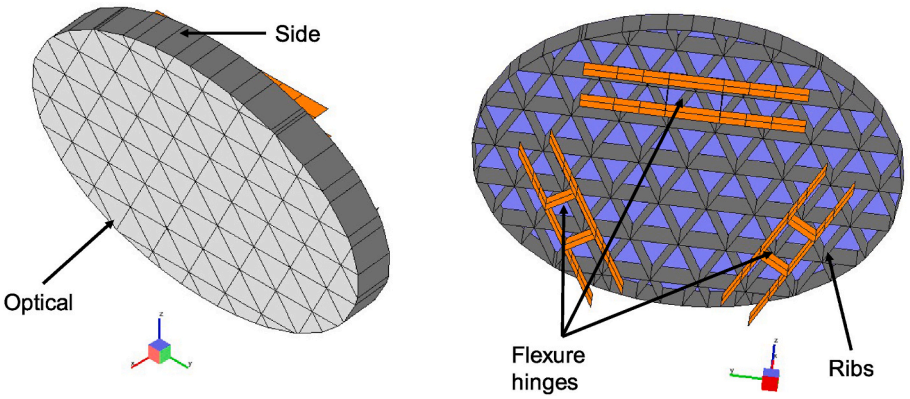

Fig. 9. Front and rear view of the Telescope Primary Mirror GMM.

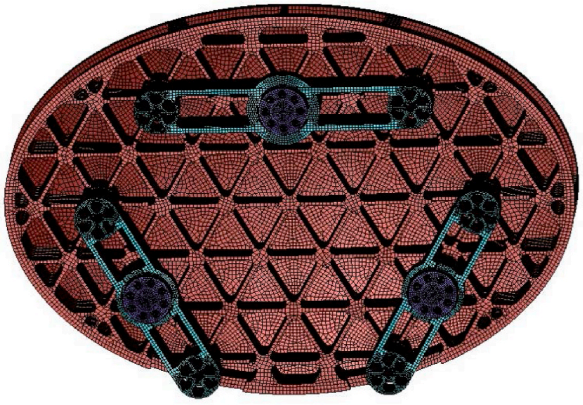

Fig. 12. FEM of the M1 mirror and its flexure hinges.

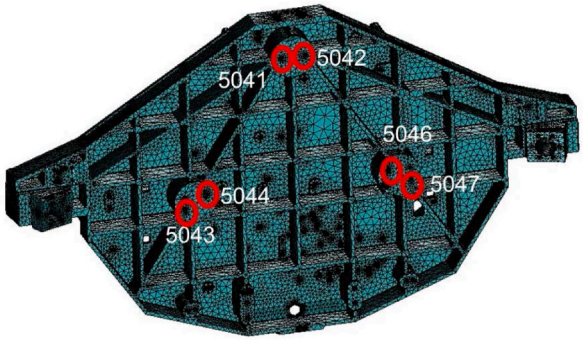

Fig. 13. Numbering range for the CBUSH elements of the TOB-Flexure hinges interface.

the temperature difference is larger, and, the infrared emissivity value of the black paint, ε, has not dropped to its cryogenic value (from $\varepsilon = 0.9$ at room temperature, to $\varepsilon = 0.55$ at cryogenic [20] temperature), resulting in a higher radiative coupling.

As previously mentioned, the temperature of the M1 during this cooling is driven by the TOB through the Flexure Hinges. Thus, naturally due to the thermal architecture, the TOB will be cooler than the Flexure Hinges which in turn will be cooler than the M1. Therefore, two thermal cases and their subsequent influence on the mechanical behaviour of the interfaces will be analysed. First, case 01, where both I/Fs, M1-Flexure Hinges and Flexure Hinges-TOB, are modelled by the contact area of each I/F, and with a contact coefficient of 100 $Wm^{-2}K^{-1}$. Second, case 02, where the conductive coupling between M1-Flexure Hinges is increased to a contact coefficient of 300 $Wm^{-2}K^{-1}$. The evolution of the average temperatures of the M1, the Flexure Hinges and the TOB interfaces along the cool-down during the first four days is represented in Fig. 14 (a) for case 01, and in Fig. 14 (b) for case 02.

It is interesting to evaluate the dynamic behaviour of the temperature gradient. To do so, it should be checked if the temperature gradient between the different parts has the same trend during cooling, or if, on the contrary, a maximum occurs at a certain temperature, and the gradient decreases.

The thermal gradient between the M1 and the Flexure Hinges parts, between the Flexure Hinges and the TOB parts, and between the M1 and the TOB parts, along the average temperature of the TOB for case 01 is represented in Fig. 15 (a), and for case 02 Fig. 15 (b). The thermal gradients have been computed by the average temperature of the thermal nodes involved in the I/F, (i.e. M1-FH I/F takes into account the thermal nodes of the six mechanical joint zones).

In both I/Fs, there is a maximum thermal gradient at a certain temperature, around ~230 K, and from that temperature, the thermal gradient decreases.

Besides, the maximum total gradient between M1-TOB parts does not occur at the same instant as the maximum gradient between M1-FH, and FH-TOB. Hence, it would be worthwhile to analyse the maximum temperature gradient at each local I/F. Then, the maximum local temperature gradient at each I/F is compared for case 01 in Fig. 16 (a), and for case 02 in Fig. 16 (b) along the average temperature of the TOB with regard to the previous average thermal gradient (the new thermal gradients have been computed taking into account only the thermal nodes involved in each local I/F).

Although the temperature gradient in each local I/F is quite similar to the global one, there is a difference of the order of magnitude of 1 K or 2 K depending on the approach followed to compute the thermal gradient. In addition, the displacement at the instant at which the maximum temperature gradient occurs, will provoke different temperature maps, as shown in Fig. 17, where the temperature map corresponding to the instant at which the maximum gradient between M1-TOB parts and M1-FH Y− I/F occurs is represented. There is a difference of 15 K in the M1 temperature depending on the approach followed. Hence, the worst-case approach followed from the thermal point of view will have an influence on the slippage analysis.

4.3. *Correlation of the analytical model for thermoelastic shear force calculation*

The aim of this section is to correlate the generated shear force, F_Q, in a joining element (bolt) that connect two parts as a function of the temperatures of both parts from the detailed FEM model with the analytical Eq. (9). In particular, the complex FEM composed of the

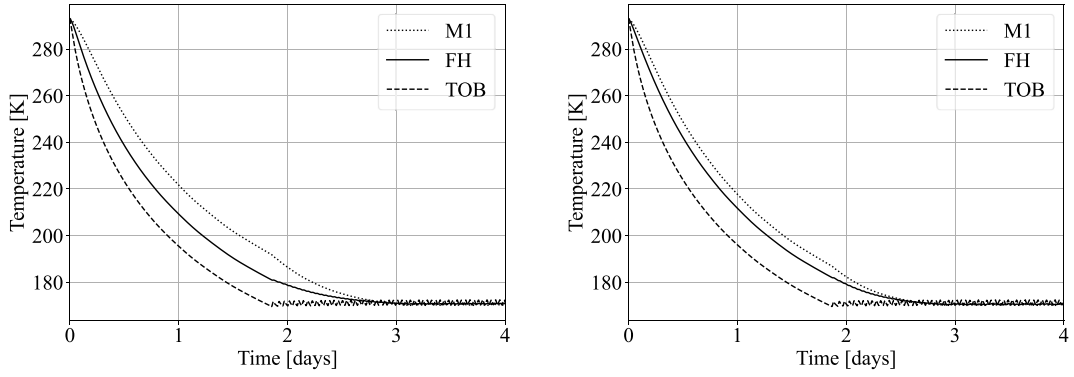

(a) Case 01. (b) Case 02.

Fig. 14. Evolution of the M1, Flexure Hinges and TOB average temperature during cool-down.

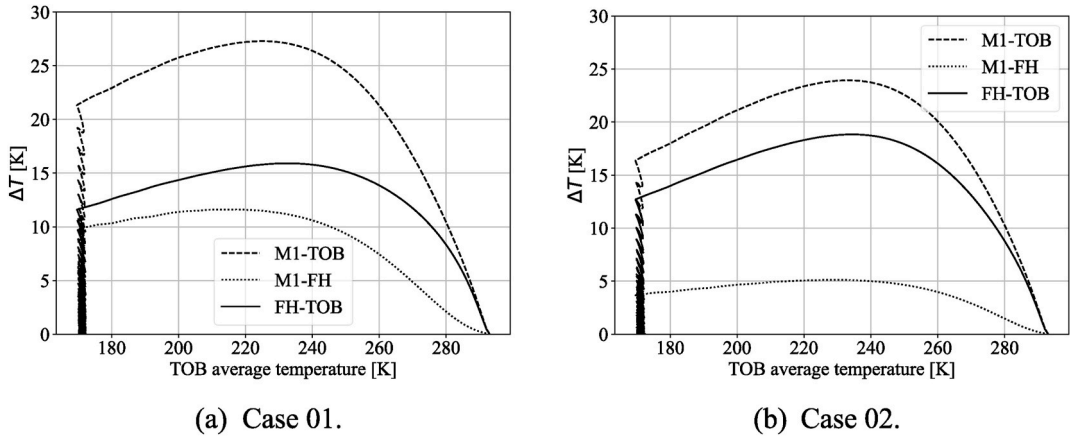

Fig. 15. Evolution of the temperature gradient along TOB average temperature during cooldown.

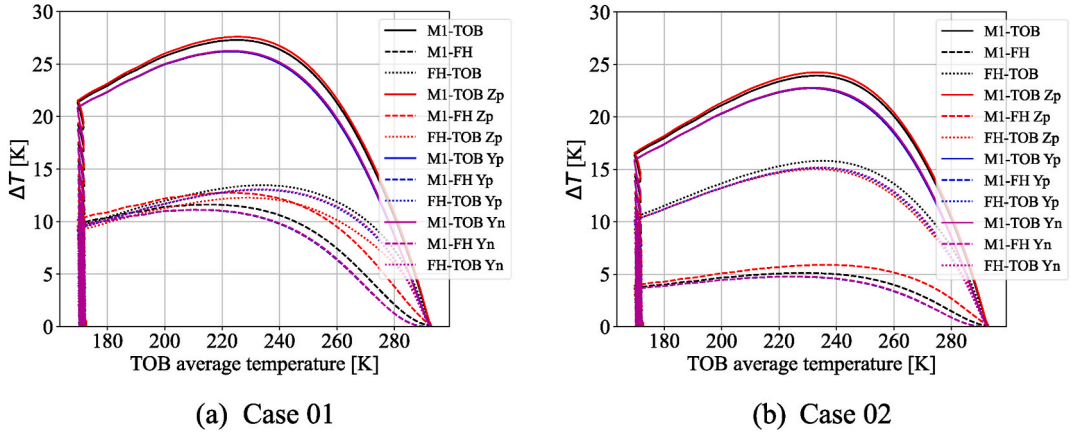

Fig. 16. Evolution of the temperature gradient along M1 average temperature during cooldown.

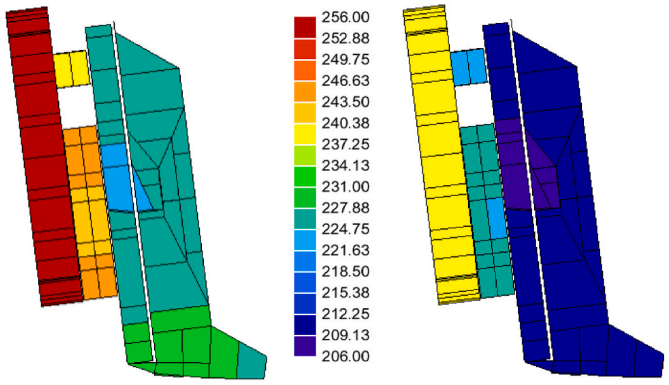

Fig. 17. Temperature map for the M1, FH and TOB units at the maximum gradient between M1 and TOB (left), and between FH-TOB Y−(right).

Optical Bench, M1 mirror and its flexure hinges (see 4.1.2) is used for this correlation, adjusting the parameter A_{eq} calculated for each I/F to provide the best correlation in each case. The rest of parameters are known as these parts are aluminium ($E_{eq} = E_{c1} = E_{c1} = 68.9$ GPa, $T_{ref} =$ 293 K), where the CTE functions of each clamped part is calculated as a function of the corresponding temperatures, considering Eq. (2) with the coefficients for the Al 6061-T6 indicated in Table 2.

In this study, several thermoelastic cases have been numerically analysed by different combinations of temperatures in the involved parts. These cases are classified in two sets of analysis (A and B).

Table 3
Input conditions of the thermoelastic analyses of the Set A for the validation of the shear force analytical equation.

Case	Input temperatures T_i [K]			Temperature differences ΔT [K]	
	TOB	Flexures	M1	TOB – Flexures	Flexures – M1
A01	236	249	254	13	5
A02	236	249	256	13	7
A03	236	251	256	15	5
A04	236	251	258	15	7
A05	236	251	260	15	9
A06	236	251	262	15	11
A07	236	251	264	15	13
A08	236	252	262	16	10
A09	236	252	264	16	12
A10	236	253	258	17	5
A11	236	253	260	17	7
A12	236	253	262	17	9
A13	236	253	264	17	11
A14	236	253	266	17	13
A15	236	254	264	18	10
A16	236	254	266	18	12
A17	236	256	264	20	8
A18	236	256	266	20	10

For each load case of the Set A (see Table 3), each part (M1 mirror, TOB) or group of similar parts (flexure hinges) has a constant temperature, but different from the temperature of the other parts. In this way, shear forces generated on the joining elements (CBUSH) caused by the temperature differences between the parts are artificially defined. For

the proposed load cases of Set A, the temperature of the TOB is fixed to 236 K, which is the temperature for this part found in the thermal analyses when the maximum gradients are generated during the cooldown (see Fig. 16). While the temperature of the flexure hinges and M1 mirror are modified in each load case to cover a range of temperature differences in each I/F that is possible to be found in the thermal analyses of the ARIEL PLM (see Fig. 15).

The input conditions for the Set B load cases are based on the thermal analyses of a thermoelastic analysis of the ARIEL PLM, where the temperature on the TOB was 206 K in the instant with the maximum temperature difference with the M1 during the cooldown. In this set of analyses, it is proposed to have different temperatures between the top flexure hinge and the lateral flexure hinges, simulating more realist conditions similar to those found for the ARIEL thermal analyses, where the top flexure hinge was cooler than the lateral flexure hinges. The proposed combinations of constant temperatures for each part are indicated in Table 4 for the thermoelastic cases of this Set B.

The comparison of the resulting shear forces between the numerical and the analytical results, and the numerical axial forces, are represented in Fig. 18, where it is depicted separately the output from each I/F and from each set of load cases. In addition, it is shown that the axial forces, F_A, changes with non-monotonic dependence on ΔT, and is less markedly than F_Q. Besides, in some cases the F_A contribution to Eq. (11) becomes negligible with regard to F_Q.

The resulting value for the equivalent area, A_{eq}, that best correlates the analytical data with the numerical results is 400 mm^2 for the TOB-Flexure hinges I/F and 180 mm^2 for the Flexure hinges-M1 IF. It is important to define a set of cases to correlate the A_{eq} parameter that is representative. If a case similar to Set B is not available, more cases like Set A with an artificially created ΔT may be used.

As the main parts of the analysed structures are made of the same material (aluminium) with the same secant CTE function. The temperature differences in the involved parts produces small CTE differences. However, the first term inside the brackets in Eq. (9) that takes into account these CTE differences is negligible compared to the second term, which shows the effect caused directly by the temperature difference between the connected parts. Therefore, this generates a quasi-linear dependency of the resulting shear forces with the corresponding ΔT, as it is appreciable from the graphs of Fig. 18, which is approximated by the following expression:

$$F_Q \simeq A_{eq} E_{eq} CTE_{c2} \Delta T \tag{13}$$

And, then Eq. (11), which determines the positive margin for slippage, is rewritten to:

$$MoS_{slip} = \frac{\left[F_{V,min} + \frac{L_c}{\delta_c+\delta_b}(CTE_{c1} - CTE_b)(T_1 - T_{ref}) - (1-\Phi_n)F_A\right]\mu_s}{sf_{slip} A_{eq} E_{eq} CTE_{c2} \Delta T} - 1. \tag{14}$$

For each interface, the axial force, F_A, is set to a representative constant value based on the order of magnitude obtained in the various numerical validation analyses. Besides, the maximum axial force for each interface has a non-monotonic dependency with the different temperature combinations as it is shown in Fig. 18.

Table 4
Input conditions of the thermoelastic analyses of the Set B for the validation of the shear force analytical equation.

Case	Input temperatures T_i [K]				Temperature differences ΔT [K]	
	TOB	Lateral flexures	Top flexure	M1	TOB – Lateral flexures	Top flexures – M1
B01	206	228.3	223.6	236	22.3	12.4
B02	206	213.8	209.5	221	7.8	11.5
B03	206	217.9	214.9	221	11.9	6.1
B04	206	215	213	218	9	5
B05	206	218	210	222	12	12
B06	206	215	213	222	9	9
B07	206	215	213	223	9	10

4.4. Evaluation of the preload force loss

The minimum preload that guarantees slippage margin positive (see Eq. (11)) of the bolts is evaluated for each I/F. The values of the parameters needed for the analytical approach are indicated in Table 5 for both interfaces. The calculation of these parameters is based on the ECSS guidelines for threaded fasteners [9], taking into account the detailed geometrical design of both interfaces. The CTE functions are based on Eq. (2), considering the constants indicated in Table 2 associated to the corresponding materials for the clamped parts (aluminium) and bolts (Inconel). It is assumed that the mechanical characteristics of the aluminium alloys used for the ARIEL TA parts (EN AW 6061-T651 and EN AW 6061-T652) are the same as those of the EN AW 6061-T6. As explained in section 4.3, the axial force, F_A, has a negligible dependence with the temperature. Therefore, a representative maximum value from these analyses is used for each interface as a constant, which are also shown in Table 5.

The preload parameter that directly appears in Eq. (10) is the minimum preload at the reference temperature of 293 K ($F_{V,min}$). The bolts for both analysed interfaces are special stud bolts. Unlike the common bolts where the preload is a consequence of the applied torque, for the stud bolts the preload is directly measured by the assembly tool during the installation of these bolts. Consequently, there is a significantly higher level of accuracy in knowing the applied preload of the stud bolts compared to the usual screws. The assembly tool used for these stud bolts guarantees that maximum applied preload during its installation do not overpasses a selected value ($F_{V,max}$), but it can be lower than this value within a certain range, which is 20 % of the maximum preload. Therefore, the minimum preload that can appear during the real assembly and is used in this evaluation ($F_{V,min}$) corresponds to the 80 % of the maximum preload.

When selecting the preload for a fastener assembly, it is essential to consider a range of design requirements beyond just the bolt analysis. Apart from evaluating the generated stresses on both the bolt and the clamped parts through the calculation of various margins as indicated in Ref. [9], several other critical aspects must be taken into account. Aspects such as the deformation caused by the preloads on the reflective surface of the mirror and on the interface plane between the instruments and the TOB, and the maximum preload that could provide the assembly tools should be considered for the selection of the maximum preload. For the analysed interfaces, the maximum allowable preloads for each interface considering the different mentioned aspects are indicated in Table 6.

Taking into account these aspects, the most restrictive maximum preload for each interface will be considered as the maximum limit for the proposed preload. Considering that the minimum preload is the 80 % of the corresponding maximum preload, the maximum limits for the minimum preloads are 52320 N for the TOB-Flexure hinges I/F and 21760 N for the Flexure hinges-M1 IF.

Finally, for different options of minimum preload at reference temperature, $F_{V,min}$, the ΔT_{lim} that avoids slippage during the cooldown is determined by equalling Eq. (11) to zero and represented in Fig. 19, based on the parameters described in Table 5.

4.5. Selection of preload based on the maximum expected temperature differences at the interfaces

The thermal gradient between the two connected parts obtained from the thermal cases described in section 4.2 is compared with the maximum allowable temperature gradient, ΔT_{lim}, at the different options of minimum preload at reference temperature, $F_{V,min}$, analysed in Fig. 19. The comparison of these curves is represented in Fig. 20, where

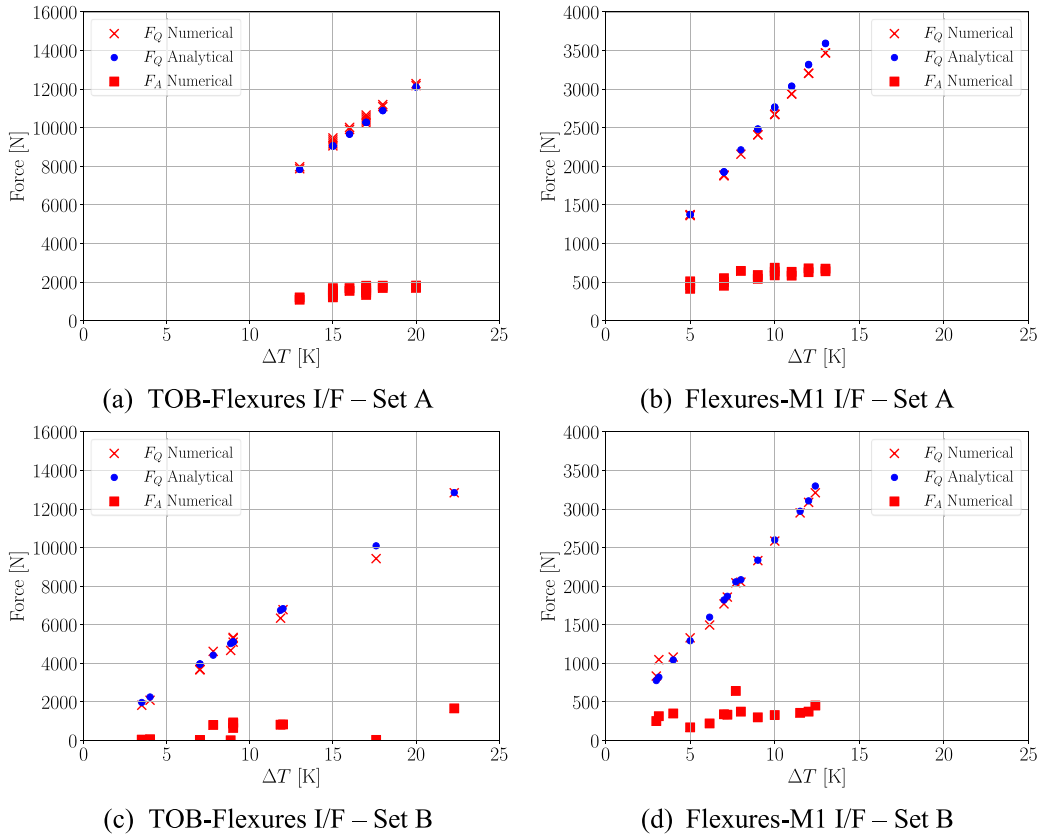

Fig. 18. Comparison between numerical and analytical shear forces, F_Q, and numerical axial forces, F_A, for the TOB-Flexures-M1 IFs.

Table 5
Values of the parameters for the analytical model to evaluate the slippage.

Parameter	TOB-Flexures IF	Flexures-M1 IF
Part 1	TOB	Flexure hinges
Part 2	Flexure hinges	M1 mirror
Material of clamped part 1	EN AW 6061-T652	EN AW 6061-T651
Material of clamped part 2	EN AW 6061-T651	EN AW 6061-T651
Material of bolt	Inconel 718	Inconel 718
Bolt metric	M12	M8
E_{eq} [GPa]	68.9	68.9
A_{eq} [mm^2]	400	180
$L_c/(\delta_C + \delta_b)$ [MN]	6.37	4.29
Φ_n	0.110	0.132
μ_S	0.3	0.3
F_A [N]	1000	500
sf_{slip}	1.25	1.25
T_{ref} [K]	293	293

Table 6
Requirements for the maximum allowable preloads for the analysed IFs of the ARIEL TA.

Requirement	Maximum allowable preloads [N]	
	TOB-Flexures	Flexures-M1
Tightening of bolts	130000	52000
Crushing of clamped parts	82000	46000
M1 reflective surface deformation	–	33000
TOB-instruments I/F plane deformation	65400	–
Assembly tool max preload	67300	27200
Most restrictive maximum preload	65400	27200

the temperature of the corresponding Part 1 for each analysed interface (see Table 5), T_1, is selected as independent variable.

It can be seen that the trend change in the $F_{V,min}$ curves does not correspond to the maximum ΔT obtained from the thermal cases. Therefore, care should be taken when selecting the most critical load case. This fact is highlighted in Fig. 21, where the results of the thermal load case 02 for the top flexure hinge-M1 I/F are compared with two $F_{V,min}$ very similar. There is a significant difference between the maximum gradient temperature and the tangential point of the thermal case curve with the analytical curve of the ΔT_{lim} associated with a preload of 9275 N. In this example, the selection of a minimum preload of 9000 N for the bolts will give positive margins (near to zero) on slippage at the point with the maximum thermal gradient ($T_1 = 257$ K, $\Delta T_{max} = 6$ K). However, Fig. 21 reveals that during the cooldown, there will be negative margins on slippage in the temperature range between 252 and 209 K with $\Delta T < 6$ K. It is necessary to increase the minimum preload up to 9275 K to avoid slippage, which provides the tangent analytical curve shown in Fig. 21. This example highlights the importance of considering not only the point with the maximum temperature difference but also the entire cooldown curve for the evaluation of the slippage on the interfaces. This is the advantage of the proposed method, which achieves this graphical representation to facilitate the correct evaluation of the potential slippage.

Based on the analytical approach proposed in this work and the numerical results provided by the thermal and structural analyses, the selected preloads for each interface are indicated in Fig. 22 and in Table 7. The nominal preloads (indicating both the minimum and maximum expected values at reference temperature) have been selected for each interface based on the minimum values to avoid slippage on the interface during the entire cooldown process for its most severe thermal analysis. In principle, it is recommended not to give more preload than necessary, especially to reduce the negative impact on the optical

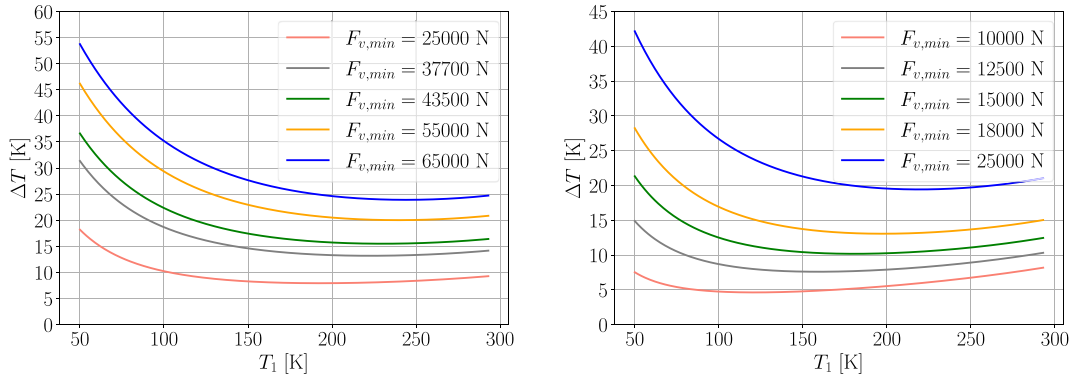

Fig. 19. Maximum allowable temperature difference to avoid slippage.

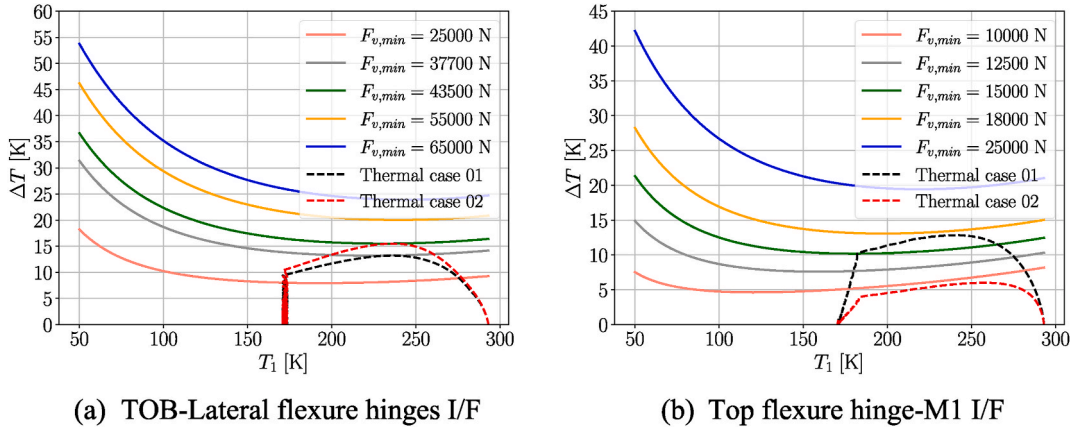

Fig. 20. Comparison of calculated temperature gradient between two clamped parts with the maximum allowable temperature difference to avoid slippage.

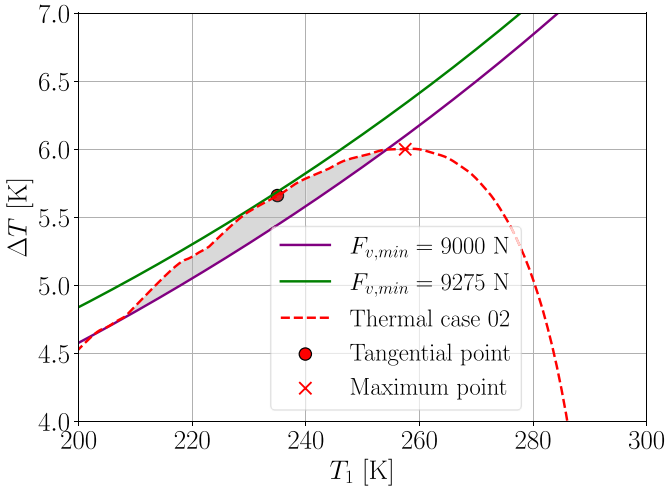

Fig. 21. Detail of the calculated ΔT from thermal case 2 for the Top flexure hinge-M1 IF.

elements due to the deformation caused by high preloads that can be problematic from optical performance point of view. It is shown that there is still a margin to increase these preloads if necessary up to the maximum limit, which is based on the most stringent requirement indicated in Fig. 22 for each I/F.

Note that these curves would slightly decrease if the bolt temperature were assumed to match that of the clamped part 2 instead of the clamped part 1 (but the overall shape would remain unchanged). As a result, the minimum allowable preload would increase, showing a more conservative approach.

4.6. *Validation of the preload selected with detailed FEM*

Several thermoelastic cases based on the flight thermoelastic cases with the non-uniform temperature distributions calculated from the two transient thermal analyses (case 01 and case 02) and explained in section 4.2 are evaluated. From each thermal analysis, four time-steps are selected based on the maximum temperature gradient at each interface, considering separately the top flexure hinge and the lateral flexure hinges. The resulting combinations of input temperatures for the thermoelastic cases define the Set C1 and Set C2, whose inputs conditions are indicated in Table 8 and in Table 9 respectively. Unlike the sets A and B (see section 4.3), for the sets C1 and C2 the temperature for each part is not constant, but with a small gradient.

The resulting equivalent area, A_{eq}, obtained in section 4.3 is used to compare the resulting shear forces obtained from the thermal maps that define de set C with the analytical results (see Fig. 23), validating the methodology.

Similarly to Fig. 22, thermal gradient curves for each I/F is represented and compared to the two proposal minimum preloads in Fig. 24, where the cases of the Set C are highlighted.

The thermal case 01 is the most severe condition for the Top flexure hinge-M1 I/F, while the thermal case 02 is the most severe for the TOB-Lateral flexure hinges. The TOB-Flexures I/F bolts with the highest thermoelastic shear forces correspond to the symmetric elements 5043 and 5047 in Fig. 13, which connect the lateral flexure hinges. On the

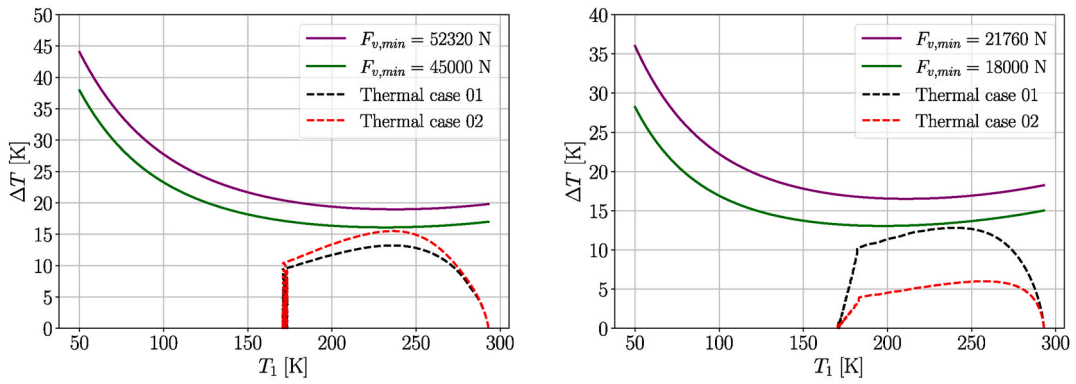

(a) TOB-Flexure hinges IF (b) Flexure hinges-M1 IF

Fig. 22. Comparison of the cooldown curves from thermal analysis and analytical curves with the selected preloads.

Table 7
Results with the selected nominal preloads for the analysed interfaces.

IF	Criterium	$F_{V,min}$ [N]	$F_{V,max}$ [N]	Max ΔT_{lim} [K]
TOB-Flexure hinges	Nominal	45000	56250	15.5
	Maximum	52320	65400	19.0
Flexure hinges-M1	Nominal	18000	22500	13.1
	Maximum	21760	27200	16.5

Table 8
Input conditions of the thermoelastic analyses of the Set C1 with the temperatures from the thermal case 01.

Case	Max ΔT time-step selection	Max temperature differences ΔT [K]			
		TOB-Top Flex	TOB-Lat Flex	Top Flex-M1	Lateral Flex-M1
C11	TOB-Top Flex	**11.6**	12.9	12.8	10.9
C12	TOB-Lateral Flex	11.5	**12.9**	12.6	10.6
C13	Top Flex-M1	11.6	12.8	**12.8**	11.0
C14	Lateral Flex-M1	11.3	12.2	12.6	**11.2**

Table 9
Input conditions of the thermoelastic analyses of the Set C2 with the temperatures from the thermal case 02.

Case	Max ΔT time-step selection	Max temperature differences ΔT [K]			
		TOB-Top Flex	TOB-Lat Flex	Top Flex-M1	Lateral Flex-M1
C21	TOB-Top Flex	**15.5**	15.3	6.0	4.9
C22	TOB-Lateral Flex	15.5	**15.3**	6.0	4.9
C23	Top Flex-M1	15.4	15.3	**6.0**	4.8
C24	Lateral Flex-M1	15.4	15.2	5.9	**4.9**

contrary, the most loaded bolts for the Flexure hinges-M1 I/F belong to those that connect the top flexure hinge due to its higher temperature difference with the M1 mirror compared to the lateral flexure hinges.

The calculation of the margins of safety on slippage by Eq. (3) for the two proposed preloads for each I/F provides the results shown in Tables 10 and 11 for the points with the maximum temperature gradient at each interface. This calculation is done based on the axial, F_A, and shear forces, F_Q, obtained from the FEM to the corresponding CBUSH element at the analysed thermal map. In addition, it is included the maximum $\boldsymbol{\Delta T_{lim}}$ obtained from the analytical model, and summarized in Table 7.

It is remarkable that in case 02, for a minimum force $F_{V,min} = 45000$ N, the obtained ΔT_{max} matches the maximum allowable ΔT_{lim}. It is notable in this case that although MoS_{slip} is positive, it is very close to zero. Additionally, in all cases where $\Delta T_{max} < \Delta T_{lim}$, MoS_{slip} remains positive, demonstrating the relevance of the proposed methodology.

The analysis carried out with the FEM model from the temperature maps of the thermal case has validated the methodology proposed in this work, obtaining for all the bolts slippage margin positive. Then, the minimum preload selected based on the analytical approach (calculated through the graphs) provides slightly positive slippage margin with the FEM model in all the interfaces, demonstrating the feasibility of the methodology proposed.

In addition, it has been pointed out that for certain interfaces, the worst-case from slippage point of view may not correspond to the maximum gradient obtained in the thermal analysis. This fact demonstrates the relevance of the proposed methodology, as it allows the slippage to be robustly evaluated during the entire transient analysed, rather than in a single case.

5. Conclusions

Thermoelastic analyses require an interaction between structural (FEM) and thermal (LPM) models to assess the effect of temperature gradients between the different parts on the mechanical behaviour. In cryogenic space telescopes, one of the worst cases from the design point of view is often during cool-down, when the different instruments go from room temperature to their cryogenic operational temperatures, generating the maximum temperature gradients during this transient process.

The aim of the work carried out in this paper is to robustly analyse the minimum preload required to guarantee that the loss of preload in the bolts during the cooling phase does not cause slippage. On the one hand, based on a very simple analytical model of each I/F under study, and after correlating the parameter, A_{eq}, with the detailed FEM model, the effect of the temperature difference between the clamped parts, the temperature at which it occurs, and the preload applied on the behaviour of each of the I/Fs from the slippage point of view is evaluated. In this way, figures of merit can be obtained to determine the potential design regions that guarantee positive slippage margins, obtaining from this study the minimum preload as a function of the temperature gradient between the clamped parts. Finally, from the temperature gradients obtained from the thermal model simulations, it is checked whether the design guarantees or not the avoid of slippage. This work has been applied to the primary mirror of the ARIEL mission as a case of study to facilitate the understanding and future use in space applications.

Therefore, thermal requirements that define the maximum thermal gradient allowable between the clamped parts can be quickly defined. In this way, the thermal design can be performed taking into account the slippage point of view from the earlier phases of the design.

Furthermore, it has been highlighted that the correct selection of the

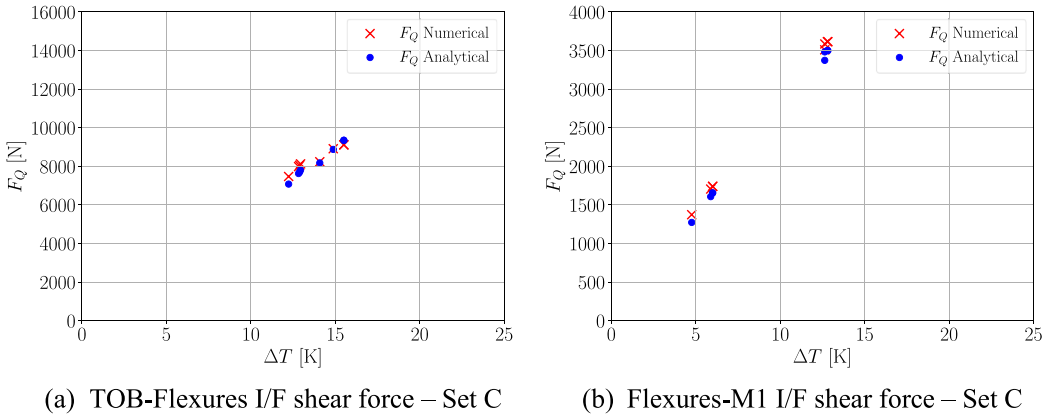

Fig. 23. Comparison between numerical and analytical shear forces for the TOB-Flexures-M1 IFs.

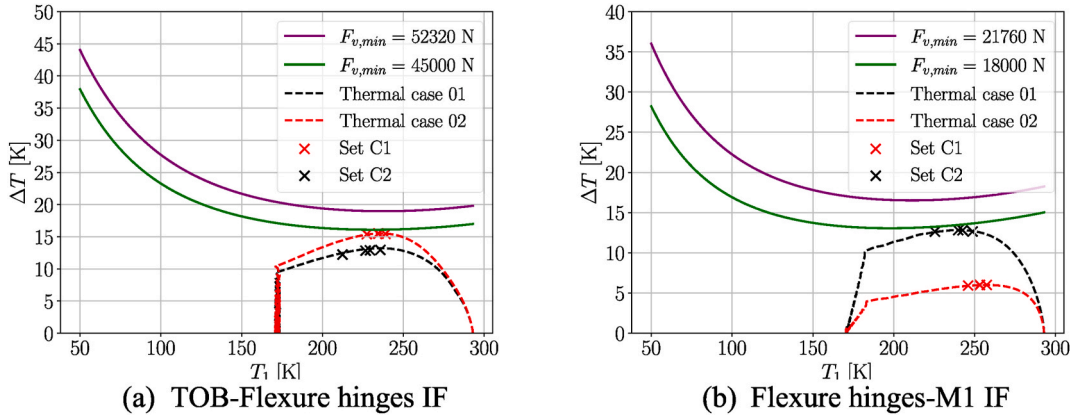

Fig. 24. Comparison of the cooldown curves from thermal analysis and analytical curves with the selected preloads.

Table 10
Margins of safety for different preloads of the TOB-Flexure hinges I/F. Thermal case 02.

$F_{V,min}$ [N]	ΔT_{max} = 15.5 K		Max ΔT_{lim} [K]
	Minimum MoS_{slip} (FEM)	Number of bolts with MoS_{slip} < 0 (FEM)	
45000	0.04	0/6	15.5
52320	0.24	0/6	19.0

Table 11
Margins of safety for different preloads of the TOB-Flexure hinges I/F. Thermal case 01.

$F_{V,min}$ [N]	ΔT_{max} = 12.8 K		Max ΔT_{lim} [K]
	Minimum MoS_{slip}(FEM)	Number of bolts with MoS_{slip} < 0 (FEM)	
18000	0.10	0/36	13.1
21760	0.35	0/36	16.5

worst thermal case for slippage analysis with the detailed FEM is the key to robustly analyse the slippage. It was shown that for certain clamped parts, the maximum gradient during the transient is not necessarily the worst case from a slippage point of view.

In addition, the importance of performing sensitivity analyses, especially of specific parameters in the thermal model, has been demonstrated. Then, the modelling parameters that play a key role in the thermoelastic behaviour in I/Fs can be identified. In this way, specific contingency plans can be designed in the early design phases, and specific tests can be scheduled if necessary, avoiding problems and delays in the following design phases.

Funding

This work has been funded by the Spanish ministry “Ministerio de Ciencia e Innovación” through project ARIEL_SCITECH with grant number PID2021-125627OB-C33.

CRediT authorship contribution statement

Alejandro Fernández-Soler: Writing – review & editing, Writing – original draft, Visualization, Validation, Software, Resources, Methodology, Investigation, Formal analysis, Conceptualization. **Andrés García-Pérez:** Writing – review & editing, Writing – original draft, Visualization, Supervision, Resources, Methodology, Investigation, Formal analysis, Conceptualization. **Gianluca Morgante:** Writing – review & editing, Supervision. **Javier Pérez-Álvarez:** Supervision. **Gustavo Alonso:** Writing – review & editing, Supervision, Funding acquisition. **Laura García-Moreno:** Writing – review & editing. **Antonio Scippa:** Writing – review & editing. **Daniele Gottini:** Writing – review & editing. **Ciro Del Vecchio:** Writing – review & editing.

Declaration of competing interest

The authors declare that they have no known competing financial interests or personal relationships that could have appeared to influence the work reported in this paper.

Acknowledgements

The authors extend their gratitude to the entire ARIEL Consortium Team for the collaborative efforts in developing the Payload Module of the ARIEL spacecraft. We particularly wish to thank our partners (RAL, INAF, UniFI, Active Space, DTU, Sener, Admatis, CEA, CBK, and JPL) for providing the various models of their respective subsystems, which were essential for integrating into the overall thermal and structural models of the ARIEL PLM. This integration was crucial for the successful completion of this work. Finally, we acknowledge the exceptional management of this project by the ESA and RAL teams.

References

[1] J. Bernard Riti, D. Dubruel, M. Nadarassin, P. Martin, E. Gavila, T. Lasic Daniel de Chambure, B. Guillaume, Planck payload module design and performance, in: http://proceedings.spiedigitallibrary.org/, 2003.

[2] S. Tuttle, L. Vaillon, U. Johann, O. Wallner, K. Ergenzinger, EUCLID mission design, in: SPIE-intl Soc Optical Eng, 2017, p. 90, https://doi.org/10.1117/12.2309226.

[3] H. Sugita, Y. Sato, T. Nakagawa, T. Yamawaki, H. Murakami, H. Matsuhara, M. Murakami, M. Takada, S. Takai, S. Yoshida, K. Kanao, Cryogenic system design of the next generation infrared space telescope SPICA, Cryogenics (2010) 566–571, https://doi.org/10.1016/j.cryogenics.2010.02.026.

[4] T. Prusti, J. De Bruijne, A.G. Brown, A. Vallenari, C. Babusiaux, C. Bailer-Jones, U. Bastian, M. Biermann, D.W. Evans, L. Eyer, et al., The Gaia mission. https://doi.org/10.1051/0004-6361/201629272, 2016.

[5] P.A. Sabelhaus, J.E. Decker, An overview of the James Webb space telescope (JWST) project, Optical, Infrared, and Millimeter Space Telescopes 5487 (2004) 550–563.

[6] S. Svendsen, E.B. Knudsen, S. Blake, T. Oosterbroek, A. Jegers, D.D.M. Ferreira, T. Prod'homme, B. Shortt, R. Willingale, P. O'Brien, Simulating the effects of thermoelastic deformation on the THESEUS Soft X-ray Imager optics, in: Optics for EUV, X-Ray, and Gamma-Ray Astronomy IX, SPIE, 2019, pp. 523–531.

[7] C. Blaurock, M. McGinnis, K. Kim, G.E. Mosier, Structural-thermal-optical performance (STOP) sensitivity analysis for the james webb space telescope, in: Optical Modeling and Performance Predictions II, 2005, pp. 246–256. SPIE.

[8] U. Garcia-Luis, A.M. Gomez-San-Juan, F. Navarro-Medina, A.E. Peláez Santos, P. Gonzalez De Chaves Fernandez, A. Ynigo-Rivera, F. Aguado-Agelet, Evaluation of the thermo-elastic response of space telescopes using uncertainty assessment, Acta Astronaut. 219 (2024) 300–317, https://doi.org/10.1016/j.actaastro.2024.03.029.

[9] ECSS Secretariat ESA-ESTEC Requirements & Standards Division, Space engineering. Threaded fasteners handbook, ECSS-E-HB-32-23A Rev.1, 2023.

[10] A. García-Pérez, G. Alonso, A. Gómez-San-Juan, J. Pérez-Álvarez, Thermoelastic evaluation of the payload module of the ARIEL mission, Exp. Astron. 53 (2022) 831–846, https://doi.org/10.1007/s10686-021-09704-0.

[11] A. García-Pérez, A. Fernández-Soler, G. Morgante, J. Pérez-Álvarez, G. Alonso, L. García-Moreno, A. Scippa, D. Gottini, R. Lilli, Temperature mapping methods for thermoelastic analyses of the ARIEL spacecraft payload module, Acta Astronaut. 223 (2024) 77–97, https://doi.org/10.1016/j.actaastro.2024.07.009.

[12] E. Pascale, P. Eccleston, G. Tinetti, The ARIEL space mission, in: 2018 5th IEEE International Workshop on Metrology for AeroSpace (MetroAeroSpace), IEEE, 2018, pp. 31–34.

[13] G. Morgante, L. Terenzi, D. D'Ascanio, P. Eccleston, M. Crook, T. Hunt, G. Tinetti, Thermal architecture of the ESA ARIEL payload, in: In *Space Telescopes and Instrumentation 2018: Optical, Infrared, and Millimeter Wave* (Vol. 10698), SPIE, 2018, July, pp. 1346–1359.

[14] Zuppella, Paola, et al. Enabling planetary science across light-years. Ariel Definition Study Report, 2020.

[15] G. Morgante, L. Terenzi, L. Desjonqueres, P. Eccleston, G. Bishop, A. Caldwell, M. Crook, R. Drummond, M. Hills, T. Hunt, D. Rust, L. Puig, T. Tirolien, M. Focardi, P. Zuppella, W. Holmes, J. Amiaux, M. Czupalla, M. Rataj, N.C. Jessen, S. M. Pedersen, E. Pascale, E. Pace, G. Malaguti, G. Micela, The thermal architecture of the ESA ARIEL payload at the end of phase B1, Exp. Astron. 53 (2022) 905–944, https://doi.org/10.1007/s10686-022-09851-y.

[16] National Institute of Standard and Technology NIST. Cryogenic Material Properties, https://Trc.Nist.Gov/Cryogenics/Materials/Materialproperties.Htm (n. d.).

[17] Simon Appel, Wijker. Jaap. *Simulation of thermoelastic behaviour of spacecraft structures*, Springer International Publishing, 2022.

[18] John D. Johnston, et al. Integrated modeling activities for the James Webb Space Telescope: structural-thermal-optical analysis. Optical, infrared, and millimeter space telescopes. Vol. 5487. SPIE, 2004.

[19] Alejandro Fernández-Soler, Gianluca Morgante, Andrés García-Pérez, Laura García-Moreno, Javier Pérez-Álvarez, Emanuele Pace, Andrea Tozi, Vladimiro Noce, Ciro Del Vecchio, Paolo Chioetto, Paola Zuppella, Thierry Tirolien, Alexandre Darrau, Lucile Desjonquères, Andrew Caldwel, Paul Eccleston, Ariel preliminary thermal decontamination study, in: 53rd International Conference on Environmental Systems, 2024. Kentucky.

[20] Martin Donabedian, American Institute of Aeronautics and Astronautics, Spacecraft Thermal Control Handbook. Volume II, Cryogenics, Aerospace Press, 2003.